ChemComm

COMMUNICATION

View Article Online
View Journal | View Issue

Cite this: *Chem. Commun.*, 2025, **61**, 14661

Received 15th June 2025,
Accepted 11th August 2025

DOI: 10.1039/d5cc03389f

rsc.li/chemcomm

Modulator-free synthesis of highly crystalline Fe-soc-C MOF and its high photocatalytic activity

Bhabani Malakar, Sudip Bhattacharjee and Asim Bhaumik *

Herein, we have successfully synthesized a modulator-free, microporous, highly crystalline cubic (100) phase of Fe-soc-C MOF *via* a solvothermal process. This material exhibited a high BET surface area (889 $m^2 g^{-1}$), microporosity, and a low bandgap (2.037 eV). This Fe-MOF showed excellent photocatalytic activity for benzimidazole synthesis and benzylamine coupling reactions under blue light.

Metal–organic frameworks (MOFs) are highly crystalline porous materials made from multidentate organic ligands connected with metal clusters.[1] They possess high BET surface area, crystallinity and low density, making them versatile for catalysis, gas storage, separation, biomedical and sensing applications.[2] In the last few decades, MOFs have attracted huge attention in photocatalysis due to their unique organic–inorganic hybrid architectures.

In MOFs there are three sites that can be used for photocatalysis: the internal void space (as they are porous in nature), the organic ligands or linkers and the uncoordinated metal clusters.[3] The organic ligands act as an antenna; they collect the incident photons and transfer the electrons from the HOMO (highest occupied molecular orbital) of the metal center to the lowest unoccupied molecular orbital (LUMO) to create a photogenerated excited state. The metal sites can function as isolated semiconductor quantum dots to absorb light and donate electrons to the ligand *via* metal-to-ligand charge transfer (MLCT). On the other hand, the π–π* transitions in the aromatic group of the organic ligand enable ligand to metal charge transfer (LMCT).[4,5] The difference in HOMO–LUMO energy determines the band gap and its value ranges from 1 to 5 eV. Because of the aromatic polycarboxylates, MOFs offer a wide range of applications for usage as photocatalysts. Due to the exceptional photoactivity of Fe–O (iron-oxo) clusters, iron-based MOFs (*e.g.*, MIL-100, MIL-53, MIL-101, MIL-88A, and MIL-88B) have been widely used for photocatalytic processes:[6–8] benzylamine oxidation reactions, polymer degradation, and benzyl alcohol oxidation reactions[9,10] are worth mentioning here.

Benzimidazole and imines are both well recognized as essential heterocyclic compounds as well as *N*-containing organic intermediates used for the synthesis of several biological, medicinal, and agricultural substances. Traditionally they are made by dehydrating an amine and condensing it with an aldehyde or ketone, these compounds suffer from low selectivity due to reactive carbonyls. Direct amine oxidation can solve this but needs costly, environmentally harmful oxidants like *tert*-butylphenylsulfinimidoyl chloride.[11] The preferred method for synthesizing these compounds would be the direct oxidation of amines by utilizing dioxygen as an oxidant.[12] It is therefore an emerging area of research to find new selective catalysts for this reaction.

The use of molecular oxygen as an oxidizing agent rather than organic peroxides is very challenging. Specifically, the synthesis of Fe-soc-C MOF ("soc" refers to square-octahedron topology) with a cubic morphology under a modulator/structure directing agent is an additional challenge. Herein, we developed the cubic phases (100) of an interesting Fe-soc-C MOF *via* solvothermal process. Again, the presence of diazo group (–N═N–) bridges enhances the planarity and π-conjugation. The azo-group also acts as a chromophore and absorbs light in the visible spectrum. So, in this work this Fe-MOF was used for several photocatalytic oxidation reactions in the presence of molecular oxygen and under mild reaction conditions. At first, we synthesized the ligand H_4ABTC *via* N═N coupling reaction and then Fe-soc-C MOF using Fe^{3+} and the H_4ABTC ligand (Fig. 1a, details in the Experimental Section, SI). Previously reported methods for the synthesis of Fe-soc-C MOF using different structure directing agents are listed in Table S1, SI.

Herein, we have modified the conventional synthesis method of Fe-soc-C MOF, which involves modulator-free synthesis. The PXRD pattern (Fig. 1b) of the sample (2–50° of 2θ) clearly matched with the previously reported simulated PXRD pattern, which confirms the bulk phase purity of the sample.[13] In order to check the porosity of the sample N_2 sorption measurement was carried out at 77 K to calculate the Brunauer–Emmett–Teller (BET) surface area. Before performing the surface area analysis, the sample was

School of Materials Sciences, Indian Association for the Cultivation of Science, 2A & 2B Raja S. C. Mullick Road, Jadavpur, Kolkata 700032, India.
E-mail: msab@iacs.res.in

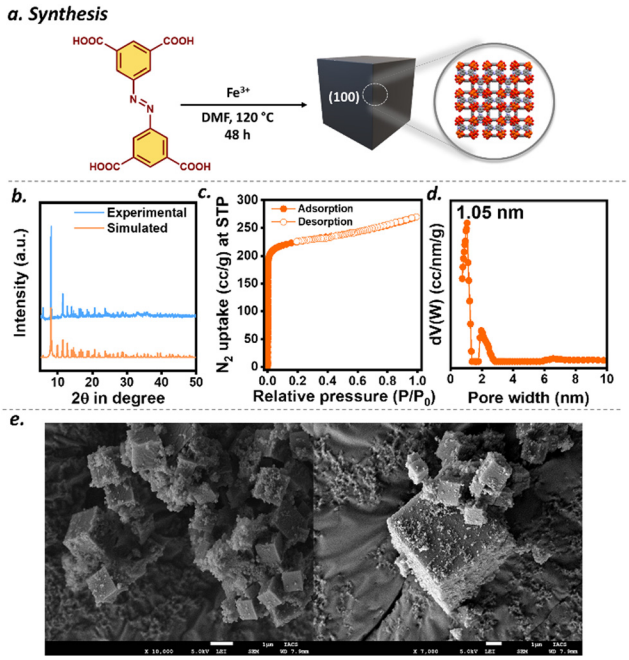

Fig. 1 (a) Schematic representation of the synthesis of Fe-soc-C, (b) simulated and experimental PXRD pattern, (c) N_2 adsorption–desorption isotherm, (d) pore size distribution plot and (e) FE-SEM images.

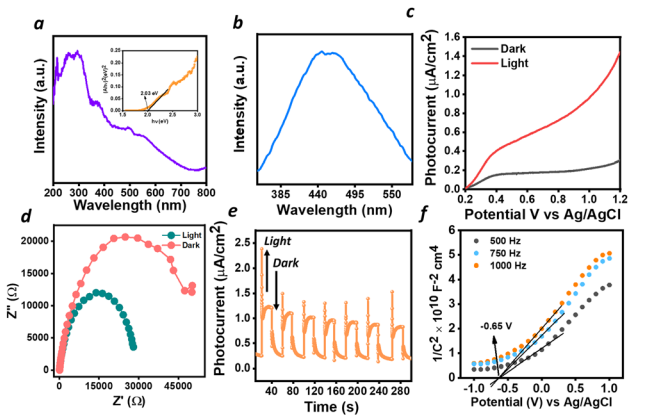

Fig. 2 (a) UV-Vis and band-gap, (b) PL-spectra, (c) linear-sweep voltammetry (under dark and light), (d) impedance spectra (under dark and light), (e) chopped chronoamperometry (under dark and light) and (f) Mott–Schottky plot of Fe-soc-C MOF.

degassed at 393 K for 4 h. The BET isotherm clearly shows that the considerable N_2 uptake in the low P/P_0 region suggests the presence of pure micropores[14] and the calculated BET surface area is 889 m^2 g^{-1} (Fig. 1c). The pore size distribution was calculated by using the NLDFT method, suggesting clear micropores of dimension 1.05 nm (Fig. 1d).[14] FTIR analysis of Fe-soc MOF (Fig. S2) showed bands at 3100–2900 cm^{-1} (aromatic-H), 1374 cm^{-1} (aromatic C), 1630 cm^{-1} (C=O), and 1574 cm^{-1} (N=N).[15] Peaks at ~620 and 540 cm^{-1} indicate Fe–O bonds in the MOF.[13,16] The material is fairly stable up to 370 °C confirmed from the thermogravimetric experiment (Fig. S3, SI). Fe-SEM images of Fe-soc-C MOF revealed cube-like crystalline morphology (Fig. 1e). From elemental mapping, the homogeneous distribution of all the elements was confirmed (Fig. S4, SI). Elemental analysis is shown in Table S2. The UV-vis DRS spectrum was collected in the range of 200–800 nm, which is shown in Fig. 2a indicating a strong absorption in the range of 500–600 nm due to ligand to metal charge transfer, while the peak at 300–200 nm is due to the π–π* transition.[17] The direct band gap is calculated to be 2.037 eV from Tauc's equation (Fig. 2a inset) and it is important to mention that this value is less than 3.1 eV, indicating the good semiconducting nature.[18] In addition, fluorescence spectra of the sample show a broad peak at 452 nm upon excitation of 320 nm, which may be attributed to the π–π* charge transfer transition between the ligand by the influence of the metal center (Fig. 2b).

To further investigate the photocatalytic properties, we have performed photoelectrochemical studies such as linear sweep voltammetry (LSV), electrochemical impedance spectra, and chopped-chronoamperometry. Fig. 2c shows the LSV plot of both in the presence of light and in the absence of light. In the absence of light, the current density was almost 0.2 μA cm^{-2} at a potential of 1.2 V *vs.* Ag/AgCl, whereas the current density increased to almost 1.4 μA cm^{-2} under the same applied potential. This sevenfold increment in current density could be attributed to the absorption of photons and photoexcited electrons and photoinduced holes. The charge transfer efficiency is also explained by the measurement of the electrochemical impedance study (Fig. 2d). The smaller radius in the presence of light compared to in the dark indicates the higher charge separation efficiency. The photocurrent response was also checked through chopped-chronoamperometry under a potential of 1.5 V *versus* Ag/AgCl. The photocurrent density increased by applying light divulging rapid e–h separation. In order to get a better understanding of the band-edge potential, Mott–Schottky analysis was performed. The positive slope in the $1/C^2$ *vs.* applied potential plot indicates the n-type semiconductor nature. The flat-band potential (E_{fb}) was calculated from the $1/C_{sc}{}^2$ *vs.* potential plot at the point where $1/C_{sc}{}^2 = 0$, and it shows −0.67 V *vs.* Ag/AgCl; −0.473 V *vs.* NHE. The calculated conduction band (CB) potential is −0.573 V (CB = E_{fb} − 0.1 V) and the valence band potential is 2.61 V *vs.* RHE (VB – CB = E_g). The oxygen activation ability of the catalyst was checked through electro paramagnetic resonance spectroscopy (Fig. 2e). After activation of oxygen in the presence of light, catalyst and solvent (Experimental section, SI), we have used 2,2,6,6-tetramethyl-4-piperidone (TEMP) as a radical trapping agent and sacrificial molecule. It shows a signal in EPR spectroscopy of TEMP-$^1O_2$ at 77 K (Fig. 2f) confirming the formation of singlet oxygen. So, this catalyst is capable of oxygen activation and reactive oxygen species formation.

As this MOF exhibits a lower band gap, a good response in photocurrent and the ability to activate oxygen, we have explored its photocatalytic activity in benzimidazole synthesis *via* oxidative coupling of *o*-phenylenediamine and aldehyde in the presence of oxygen and MeCN as a solvent. Benzimidazole derivatives are highly important chemicals because of their pharmacological and biological applications.[19] In this study *o*-phenylenediamine and benzaldehyde are taken as a model

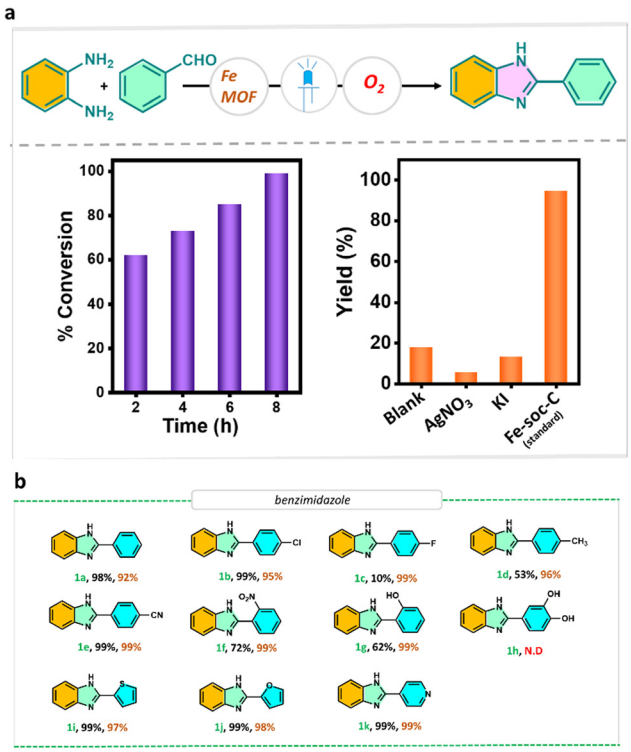

Fig. 3 (a) Photocatalytic activity of Fe-soc-C for benzimidazole synthesis and optimization study, (b) substrate scope. Conversions were calculated using GC-MS analysis (conversions were indicated in black and selectivity was indicated in red).

substrate and then we have performed the reaction under blue light (427 nm) irradiation in the presence of an oxygen environment. Before performing the catalytic reaction, a blank test was performed, which showed lower product yield. The conversion was monitored using GC-MS analysis and the formation of the product was confirmed using ^{1}H NMR analysis. In addition to the main product, a side product also formed. After 8 h of reaction, we observed that all the reactant molecules are consumed and benzimidazole formed exclusively (Fig. 3a). To identify the reactive species, the reaction was performed in the presence of different scavenging agents. In the presence of $AgNO_3$ as an electron scavenger, the yield gradually decreased, indicating the formation of photogenerated electrons. Again, the yield decreased upon the addition of KI, clearly indicating the formation of photogenerated holes. So, upon irradiation of light, the e-h separated rapidly in this reaction. We then tested the catalytic activity towards a series of substrates, which are shown in Fig. 3b. Most of the substrates show maximum conversion with high selectivity, except for the 4-F containing substrate, which may be due to the electronegative effect of fluorine in the *para* position.

We further conducted the catalytic experiments for benzylamine oxidation in the presence of blue light.[20,21] In our previous study, we observed that MeCN was the best solvent for this transformation.[22] In 2 h of reaction we observed that the conversion was 33.7%. With increasing time, the yield gradually increased to 60.6% after 6 h and the total benzylamine was converted after 10 h (products were analysed by GC-MS and ^{1}H NMR). Furthermore, the catalytic experiment was evaluated under different intensities of light, which is shown in Fig. S5, SI. This benzylamine coupling reaction proceeds under blue light irradiation at room temperature. We have started our experimentation with benzylamine as a model substrate in the presence of an oxygen environment. This reaction is possible only two ways: one is the elimination of ammonia and the other is *via* the formation of benzaldehyde, which is shown in the mechanism. In the ^{1}H NMR analysis we observed derivatives of benzaldehyde as a side product. A series of substrates have been tested, which are mentioned in Fig. 4b. Less conversion was observed when an electronegative group was present in the *para* position.

The probable mechanism for both the photocatalytic reactions over Fe-soc-C MOF is shown in Fig. 5. In both reactions, the activation of oxygen and formation of reactive oxygen species is important. The mechanistic pathway shows the involvement of $O_2^{\bullet-}$ and $^1O_2$ as reactive oxygen species. To check the formation of $O_2^{\bullet-}$ species 5,5-dimethyl-1-pyrroline *N*-oxide (DMPO) was used as a trapping agent and EPR analysis was performed in both 77 K and at room temperature, respectively. In this study we did not get any typical signal of DMPO–$O_2^{\bullet-}$ species at room temperature. However, we observed a typical signal of DMPO–$O_2^{\bullet-}$ at 77 K which may be due to the lower concentration of $O_2^{\bullet-}$ (Fig. S7, SI).[23] Furthermore, we observed the typical signal of TEMPO at room temperature as well as 77 K with high intensity, indicating high concentration of $^1O_2$ in the system.[24] Again, the singlet oxygen species was confirmed through oxidation of 1,3-diphenylisobenzofuran (DPBF), which is a classical sacrificial agent of singlet oxygen. The decrease in intensity with time of the distinguished absorption band of DPBF (Fig. S6, SI) at 410 nm indicates the

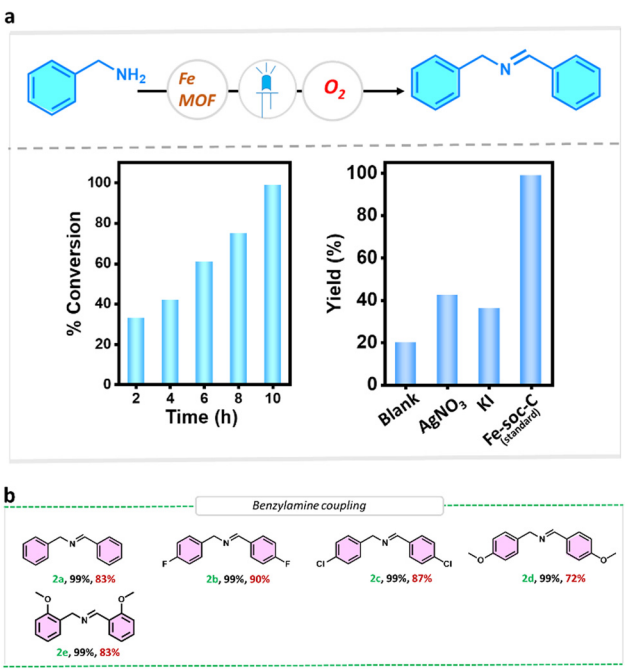

Fig. 4 (a) Photocatalytic activity of Fe-soc-C for benzylamine coupling and optimization study, and (b) substrate scope. Conversions were calculated using GC-MS analysis (conversions were indicated in black and selectivity was indicated in red).

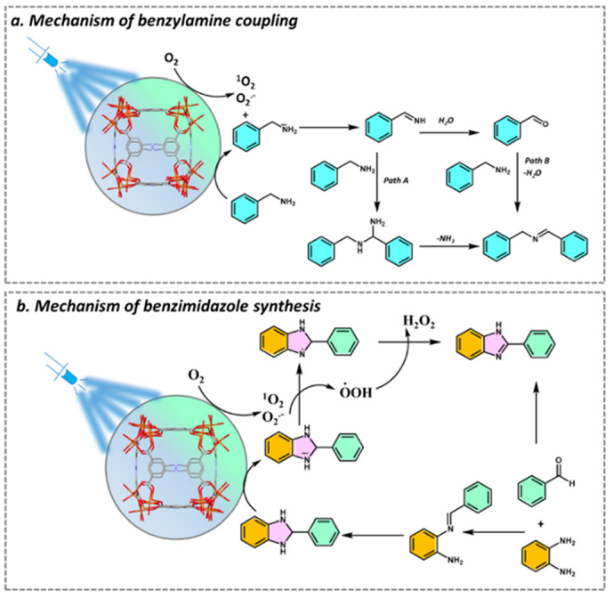

Fig. 5 Probable reaction mechanism of (a) benzylamine coupling reaction and (b) benzimidazole synthesis over Fe-soc-C MOF.

oxidation of DPBF by the singlet oxygen. The stability of the catalyst was further assessed through PXRD and FT-IR analysis (Fig. S8 and S9, SI), which revealed that there was no structural change up to four cycles. Tables S3 and S4, SI highlight the superiority of Fe-soc-C MOF for both the reactions in comparison to the state-of-the-art catalysts. The amount of catalyst loading for other cases was high in comparison to our catalytic systems.

In conclusion, we have reported a new synthetic method for the cubic Fe-soc-C MOF without using any modulator. This Fe-MOF with a very low band gap displayed excellent photocatalytic activity for the benzimidazole synthesis and benzylamine coupling reactions. Thus, our result may open new avenues for eco-friendly photocatalysis in the future.

B. M. wants to thank UGC, New Delhi for a Junior Research Fellowship. S. B. would like to thank IACS, Kolkata for a Senior Research Fellowship. A. B. would like to thank DST-SERB for a Core Research Grant (project no. CRG/2022/002812).

Conflicts of interest

There are no conflicts to declare.

Data availability

The data supporting this article (ligand, MOF synthesis, TGA, FTIR, EPR, NMR and GCMS of products, comparison tables) have been included in the SI. See DOI: **https://doi.org/10.1039/d5cc03389f**

Notes and references

1 (*a*) N. W. Ockwig, O. Delgado-Friedrichs, M. O'Keeffe and O. M. Yaghi, *Acc. Chem. Res.*, 2005, **38**, 176; (*b*) X. R. Li, X. C. Yang, H. G. Xue, H. Pang and Q. Xu, *EnergyChem*, 2020, **2**, 100027.
2 (*a*) S. NavalÓn, A. Dhakshinamoorthy, M. Álvaro, B. Ferrer and H. GarcÍa, *Chem. Rev.*, 2023, **123**, 445–490; (*b*) S. Chongdar, S. Bhattacharjee, P. Bhanja and A. Bhaumik, *Chem. Commun.*, 2022, **58**, 3429–3460; (*c*) S. P. Tripathy, S. Subudhi and K. Parida, *Coord. Chem. Rev.*, 2021, **434**, 213786; (*d*) A. M. Bumstead, C. Castillo-Blas, I. Pakamorė, M. F. Thorne, A. F. Sapnik, A. M. Chester, G. Robertson, D. J. M. Irving, P. A. Chater, D. A. Keen, R. S. Forgan and T. D. Bennett, *Chem. Commun.*, 2023, **59**, 732–735.
3 S. Subudhi, D. Rath and K. M. Parida, *Catal. Sci. Technol.*, 2018, **8**, 679–696.
4 L. V. Bora and R. K. Mewada, *Renewable Sustainable Energy Rev.*, 2017, **76**, 1393–1421.
5 L. V. Meyer, F. Schonfeld and K. Müller-Buschbaum, *Chem. Commun.*, 2014, **50**, 8093–8108.
6 M. H. Beyzavi, N. A. Vermeulen, A. J. Howarth, S. Tussupbayev, A. B. League, N. M. Schweitzer, J. R. Gallagher, A. E. Platero-Prats, N. Hafezi, A. A. Sarjeant, J. T. Miller, K. W. Chapman, J. F. Stoddart, C. J. Cramer, J. T. Hupp and O. K. Farha, *J. Am. Chem. Soc.*, 2015, **137**, 13624–13631.
7 D. Yang and B. C. Gates, *ACS Catal.*, 2019, **9**, 1779–1798.
8 S. M. J. Rogge, A. Bavykina, J. Hajek, H. Garcia, A. I. Olivos-Suarez, A. Sepúlveda-Escribano, A. Vimont, G. Clet, P. Bazin, F. Kapteijn, M. Daturi, E. V. Ramos-Fernandez, F. X. Llabrési Xamena, V. Van Speybroeck and J. Gascon, *Chem. Soc.*, 2017, **46**, 3134–3184.
9 G. Férey, C. Mellot-Draznieks, C. Serre, F. Millange, J. Dutour, S. Surble and I. Margiolaki, *Science*, 2005, **309**, 2040–2042.
10 Z. Wang, P. Yeary, X. Feng and W. Lin, *J. Am. Chem. Soc.*, 2023, **145**, 8647–8655.
11 T. Mukaiyama, A. Kawana, Y. Fukuda and J. Matsuo, *Chem. Lett.*, 2001, **30**, 390–391.
12 M. Deb, S. Hazra, P. Dolui and A. J. Elias, *ACS Sustainable Chem. Eng.*, 2019, **7**, 479–486.
13 A. J. Cairns, J. Eckert, L. Wojtas, M. Thommes, D. Wallacher, P. A. Georgiev, P. M. Forster, Y. Belmabkhout, J. Ollivier and M. Eddaoudi, *Chem. Mater.*, 2016, **28**, 7353–7361.
14 M. I. Severino, A. A. l Mohtar, C. V. Soares, C. Vieira, O. Kolmykov, C. Freitas, I. Dovgaliuk, C. Martineau, V. Pimenta, F. Nouar, G. Maurin, M. L. Pinto and C. Serre, *J. Mater. Chem. A*, 2023, **11**, 4238–4247.
15 B. Malakar, S. Bhattacharjee, N. Q. M. Tran, D. T. Le Hoang, T. B. Phan, S. Chongdar and A. Bhaumik, *Chem. Commun.*, 2025, **61**, 81–84.
16 Z. J. Chen, X. J. Wang, R. Cao, K. B. Idrees, X. Y. Liu, M. C. Wasson and O. K. Farha, *ACS Mater. Lett.*, 2020, **2**, 1129–1134.
17 S. Rojas and P. Horcajada, *Eur. J. Inorg. Chem.*, 2021, 1325–1331.
18 S. Bhattacharjee, S. Bera, R. Das, D. Chakraborty, A. Basu, P. Banerjee, S. Ghosh and A. Bhaumik, *ACS Appl. Mater. Interfaces*, 2022, **14**, 20907–20918.
19 B. Narasimhan, D. Sharma and P. Kumar, *Med. Chem. Res.*, 2010, **21**, 269.
20 S. Furukawa, Y. Ohno, T. Shishido, K. Teramura and T. Tanaka, *ACS Catal.*, 2011, **1**, 1150.
21 P. Eskandari, Z. Zand, F. Kazemi and M. Ramdar, *J. Photochem. Photobiol., A*, 2021, **418**, 113404.
22 S. Bhattacharjee, S. Mondal, A. Ghosh, S. Banerjee, A. K. Das and A. Bhaumik, *Small*, 2024, **20**, 2406723.
23 A. Chakraborty, A. Alam, U. Pal, A. Sinha, S. Das, T. Saha Dasgupta and P. Pachfule, *Nat. Commun.*, 2025, **16**, 503.
24 X. W. Zhang, Z. Li, N. Ta and H. X. Han, *ACS Sustainable Chem. Eng.*, 2022, **10**, 4059–4064.

